Real-time Monitoring of Laser Beam Welding Using Infrared Weld Emissions

P. G. Sanders, J. S. Keske, G. Kornecki, and K. H. Leong
Technology Development Division
Argonne National Laboratory
Argonne, IL 60439
USA

Abstract

A non-obtrusive, pre-aligned, solid-state device has been developed to monitor the primary infrared emissions during laser welding. The weld monitor output is a 100-1000 mV signal that depends on the beam power and weld characteristics. The DC level of this signal is related to weld penetration, while AC portions of the output can be correlated with surface irregularities and part misalignment or contamination. Changes in DC behavior are also noted for both full and deep penetration welds. Full penetration welds are signified by an abrupt reduction in the weld monitor output. Bead on plate welds were made on steel, aluminum, and magnesium with both a CW CO_2 laser and a pulsed Nd:YAG laser to explore the relationships between the weld characteristics and the weld monitor output.

KEYWORDS: laser welding; infrared; process monitoring; penetration

Introduction

The use of laser beam welding in industrial processes has increased significantly in recent years. Compared to conventional arc-welding, laser beam welding allows higher process speeds, better precision, and smaller heat affected zones. Although cost has traditionally been a limitation to the installation of laser welding stations on the factory floor, consideration of all manufacturing costs and production requirements usually reveals that laser welding is competitive. The increased power and lower prices of new laser systems is continually enhancing the competitive position of laser welding. As the use of laser welding technology increases, so does the need for reliable methods for process monitoring.

There are several characteristic signals associated with the laser beam welding process. If a laser beam of sufficient irradiance to melt the metal is focused at or into the surface of the work piece, a keyhole is formed. This keyhole within the molten metal is sustained by the evaporation of metal from the weld pool. The outward flow of this metallic vapor from the keyhole produces acoustic waves. Plasma is formed within and above the keyhole by ionization of the shielding gas and the metallic vapor. The primary signal from the welding process is the infrared emissions from the weld pool. Secondary signals include the radiation from the plasma (primarily in the visible and ultraviolet region) and the acoustic waves. Most weld monitoring methods sense at least one of these signals.

Variations in the plasma or acoustic emissions may indicate changes in weld quality, but monitoring these secondary signals tends to be difficult, complex, and expensive to implement. On the other hand, primary infrared emissions simply indicate the heat content of the weld. For example, deeper penetration tends to correlate with increased heat input (caused by higher laser beam irradiances or slower travel speeds). Greater heat input results in higher temperatures and increased infrared emissions. The temperature may be monitored by a pyrometer, but this is difficult due to the slow response time of the system and the presence of an intense thermal signal from the plasma inside the keyhole. A better indicator is the infrared energy emitted by the weld, including both the contributions from the hot molten metal and the keyhole plasma. The ultraviolet and visible contributions may be minimized by selecting an infrared detector having a maximum sensitivity in the range of the molten metal emissions.

Using Wien's law ($\lambda_{max} = 2898/T$), the wavelength (μm) with the maximum radiant energy may be estimated at a specific temperature (K). For the case of steel, which is liquid from about 1800 to 3100 K, the wavelength of interest for weld monitoring would be in the near infrared (from 1.6 to 0.9 μm). Due to the higher temperature and characteristic emissions of the keyhole plasma, the majority of the radiant energy is at shorter wavelengths in the visible and ultraviolet range.

Researchers have implemented various forms of weld monitors (1-7). Most have used combinations of infrared and ultraviolet sensors or several infrared sensors. Chen et. al. (1) correlated infrared and ultraviolet signals from above the weld with variations in weld quality (related to surface condition, dropout, and gas shielding) and observed that the weld signal increased with increasing laser power and decreasing travel speed. Bagger et al. (2), Olsen et al. (3), and Chang (4) have used infrared detectors above and below the weld to detect full penetration. Bagger et. al. also noted variations in signal levels with laser power and shielding gas flow rate. Maischner et al. (5) (plasma above weld) and Mori and Miyamoto (6) (two infrared sensors above weld) have both noted that the AC signal variation increases when the weld fully penetrates the work piece. Nava-Rüdiger and Houlet (7) have used two infrared detectors above the weld to detect geometric defects such as sagging or part misalignment.

The design objectives for the weld monitoring device in this paper are that it be low cost, robust, and rugged. The robustness of the device is related to the ease of data analysis and the a minimization of mistagged welds. To be rugged, the weld monitor must reliably operate in the harsh manufacturing environment. The weld monitor output is represented in an intuitive graphical format, in which the data is completely represented by a plot of voltage versus time. The primary infrared weld signal is monitored by one sensor integrated into the optics (8), which greatly simplifies collection and analysis of the data. The infrared detector collects emissions from directly above the weld, and does not require sensors beneath the weld. Integration of the detector into the optics makes the system very compact and less susceptible to bumping or misalignment. This monitoring concept has been incorporated into transmissive or reflective optics on both CO_2 and Nd:YAG lasers.

Experimental Methods

Welds were made at travel speeds between 5 and 15 cm/s width a 6 kW CW CO_2 laser (Rofin Sinar RS6000) using a near TEM_{20} and a 150 mm off-axis parabola. The focused beam diameter was ≈ 400 μm with an M^2 of 4.1. The power was varied from 0.5 to 5.5 kW to produce mean irradiances ranging from 0.25 to 3.5 MW/cm^2. The mean irradiance corresponds to the ratio of 86% of the power over the cross-sectional area containing 86% of the power. Bead on plate welds with focus on the surface were made on steel sheet and plate stock (1020 and 1045) as well as aluminum (6061) and magnesium (AZ31) sheet. Top gas shielding was provided by a 50 lpm flow

of helium in a trailing jet configuration delivered by a 0.5 cm diameter tube oriented at 45° from the surface and 1 cm from the weld.

Additional welds were made on a pulsed 1.6 kW Nd:YAG laser (Electrox) with a 1000 μm fiber and a 75 mm transmissive focusing optic. Bead on plate welds were made on 1045 steel at travel speeds ranging from 1.5 to 5 cm/s. The average power was 1.2 kW (3.75 kW peak) at the work piece, in which the pulse width was 1.6 ms and the repetition rate was 200 Hz. The beam diameter was 600 μm, which produced a mean peak irradiance of 1.3 MW/cm^2. Circumferential lap fillet welds (9) were made on stainless steel at 60 rpm with an average power of 0.3 kW (1.7 ms pulse width and 190 Hz repetition rate). Top gas shielding was provided by a 40 lpm flow of argon in a trailing jet configuration delivered by a 0.8 cm diameter tube oriented at 45° from the surface and 1 cm from the weld.

For both lasers, infrared weld monitors were integrated into the optics. This implementation is stable and inconspicuous, eliminating the need for alignment or changes in the welding process. The CO_2 weld monitor utilizes a scraper mirror located on the lower corner block mirror, while the YAG assembly uses oversized, off-axis optics to collect the weld signal. Weld monitor voltages as a function of time were collected using data acquisition hardware and software (GW Instruments, Somerville, MA) with an Apple Macintosh computer. The data collection rate was between 500 and 2000 Hz. The weld monitor system noise (standard deviation) when not welding was 0.25 mV, while the AC variation due to welding ranged from 1 to 15 mV. Filtering may be used to reduce the noise level of the data, but some information may be lost in this process. After welding, the steel, aluminum, and magnesium coupons were sectioned, polished, and etched to determine weld depth, width, and surface profile.

Results and Discussion

The results are divided into three sections. In the first, the dependence of the weld monitor output on penetration depth is described. The penetration section addresses partial penetration, full penetration, and deeper penetration welds. The second part demonstrates the sensitivity of the weld monitor to defects caused by part misalignment and surface contamination. Finally, the third topic is the repeatability of the weld monitor signal and the use of the weld monitor for process control.

Penetration

The energy input per unit length was increased by increasing the laser power at constant speed or decreasing the travel speed at constant power. The increased energy input led to increased penetration and higher infrared emissions from the weld pool. An almost linear relationship was observed between the weld monitor signal and the weld penetration depth in steel and magnesium (Fig. 1a, c). Many researchers have noted the increase in the weld monitor signal with increasing power or decreased travel speed (1, 2), but few have correlated the weld monitor signal with the penetration. The penetration was varied both by changing the travel speed (steel) and the power (magnesium). The correlation between the weld monitor signal and the penetration was weaker for the aluminum (Fig. 1b), due to a combination of less variation in the DC level with penetration and a higher AC component.

Variations in the weld monitor signal with material type (steel, aluminum, and magnesium) are shown in Fig. 2. All the penetration depths were about 1 mm, and the travel speeds were ≈ 13 cm/s. The power was 3.7 kW for the steel and aluminum and 1.2 kW for the magnesium. The AC variation increased dramatically from the steel to the aluminum and magnesium. These changes may be related to greater keyhole stability in molten steel. Factors aiding keyhole stability in steel include higher absorptivity, and the higher viscosity and surface tension of the molten metal (Table 1). Opening and closing of the keyhole in aluminum and magnesium may contribute to the

oscillations in the weld monitor signal. The DC levels of the aluminum and magnesium are similar to the steel even though the melting point of steel is significantly higher (Table 1). The DC level from aluminum and magnesium may be higher due to generation of a more intense plasma when welding .

Table 1. Comparison of Physical Properties of Magnesium, Aluminum, and Iron

Property	Magnesium	Aluminum	Iron	Ref.
Melting point (°C)	650	660	1536	10
Density (g/cm^3)	1.74	2.70	7.86	10
Heat of fusion (J/g)	368	396	274	10
Specific heat (J/g °C)	0.92	1.05	0.46	10
Energy to melt (J/cm^3)	1650	2900	7650	
Absorptivity (% @ 10.6 μm)	3	5	10	11
Viscosity (mN s/m^2 @ T_{mp})	1.25	1.3	5.5	10
Surface tension (N/m @ T_{mp})	0.55	0.90	1.87	10

The weld monitor output from a pulsed YAG laser is shown in Fig. 3a. The weld monitor signal consists of essentially two levels which will be termed the upper bound and the lower bound. The upper bound of the signal occurs during the actual pulse and originates from the heating of the material and formation of plasma. Due to rapid thermal relaxation, this signal quickly decays to the lower bound after the pulse ends. This upper level of the signal is not due to reflection of the YAG beam, since it is still observed when the beam is tilted. In addition, a notch filter with an optical density of 5 at the YAG wavelength is installed in front of the weld monitor. The lower bound of the signal was related to the weld pool temperature and the penetration depth. The gradual formation of the weld pool was indicated by the rise of the lower bound of the signal during the first 0.2 s of the weld, after which the signal stabilizes. Fig. 3b shows the change in weld monitor signal with increasing depth and width of the weld. The weld penetration was changed by varying the travel speed at constant pulse parameters and average laser power, since it was difficult to vary the power without changing the pulse characteristics significantly. As the weld dimensions increased,the weld monitor signal increased, consistent with the CW CO_2 results above. The high R-squared values indicate the quality of the fit.

An abrupt drop in the weld monitor signal was observed when full penetration was achieved (Fig. 1). In all three materials, the weld monitor signal showed an increasing trend with increasing penetration until full penetration is reached. The significant drop in the weld monitor signal can be justified by noting that when the keyhole goes completely though the material, some energy is lost on the bottom side of the work piece. This has been observed by researchers who used sensors beneath the weld in their monitoring schemes (2-4). They have measured significant signals on the bottom during full penetration welding, and it appears that the top signal was correspondingly reduced. In the transition region between partial and full penetration, the DC level of the weld monitor signal is highly variable and decreases from the partial penetration maximum to the full penetration minimum.

*Higher AC components in the weld monitor signal are generally related to greater keyhole instability. Increased variation in the AC component of the weld monitor signal was observed when the keyhole fully penetrated the work piece (consistent with 5,6) and at slower travel speeds. When full penetration is obtained by varying the power, the AC variation is slightly increased over

a partial penetration weld at the same speed (Fig. 4). However, if full penetration is achieved by decreasing the travel speed, the AC component of the weld monitor signal is increased due to both full penetration and slower travel speed (Fig. 4). The average AC variations for 5 welds made at each of the conditions in Fig. 4, as measured by the standard deviation, are shown in Table 2. These AC variations are consistent with all the steel data collected. A minimum AC variation of 1 mV was obtained with shallow welds in steel at high speeds, while the maximum variation in steel is observed both at full penetration and slow travel speeds or with deeper penetration welds (≈ 5 mm).

Table 2. AC Variation in Weld Monitor Signal with Travel Speed and Penetration

	Partial Penetration	Full Penetration	Full Penetration
Weld parameters	13 cm/s, 4.3 kW	13 cm/s, 4.9 kW	6 cm/s, 3.7 kW
AC variation (mV)	1.9 ± 0.2	3.5 ± 0.3	7.0 ± 0.6

The impact of deeper penetration on the weld monitor output is shown in Fig. 5. Both increased power at constant speed and decreased speed at constant power were used to obtain the data in the plot. For the curve in which the power was increased, the weld monitor signal showed a weak correlation with depth. Considering the AC noise level at this penetration, accurate prediction of penetration is not as practical as at lower penetration levels. In the case of varying the speed, a larger change in the weld monitor signal with penetration was observed. However, as the speed was reduced, the weld width increased from 1.5 to 4.5 mm. This increase in the area from which the infrared signal originates will increase the collected signal in the same manner as an increase in penetration. It appears that at penetration depths above 2 mm, the infrared radiation emitted by the weld was not as sensitive to the weld depth. It may be more difficult for the infrared emissions from the weld to reflect the conditions deep within the material.

Weld Quality

Seams and gaps in butt welds were easily recognized in the weld monitor output. In Fig. 6 is an image of the weld made with simulated defects along with a plot of the weld monitor signal corresponding to this weld. On the left there was a seam between two pieces of metal on the top side of the butt weld. This seam produces a drop in the weld monitor signal, and this drop would increase in duration as the gap between the two pieces increased. On the right side of this butt weld, there is a gap caused by poor fit-up. This also produced an abrupt drop in the weld monitor signal, indicating incomplete bonding of the material.

The effects of rotary misalignment are demonstrated in Fig. 7. Circumferential fillet welds were made both with the part coincident (Fig. 7a) and skewed (Fig. 7b) from the rotary axis. The primary difference between the two plots is the oscillatory nature seen in the bottom portion of the weld monitor signal. This waviness was caused by the movement of the weld bead on and off the step between the two pieces of metal to be welded. Ideally, the beam would travel along the seam between the two parts. The smaller bumps on the signal in Fig. 7a were the result of surface imperfections on the weld bead.

The impact of surface contamination on the weld monitor signal have been observed on several occasions. The burning of a flammable substance such as oil on the work piece produced a weld signal with a higher DC level and a significantly greater AC component. The protective chromate coating applied to magnesium alloys led to a reduction in the AC component of the weld monitor signal. The penetration data (Fig. 1c) was from magnesium with the protective coating, while the while the weld monitor signal in Fig. 2 was from magnesium with the coating removed. The standard deviation of the weld monitor signal increased from 11 to 19 mV when the coating

was removed. This chromate coating on magnesium may aid in coupling the laser beam with the work piece, which is similar in function to coatings for laser heat treating of iron-based alloys. By knowing the normal variation in the weld monitor signal, differences in the work piece surface condition can easily be detected.

Repeatability and Process Monitoring

Variations between the weld monitor signals from individual welds made on the same day is shown in Fig. 8. This figure shows five partial penetration welds (higher DC level) and five full penetration welds (lower DC level). The reason for the drop in the DC level with full penetration was noted above. All the weld monitor traces for both conditions lie on top of each other illustrating the repeatability of weld monitor. The weld parameters for the welds in Fig. 8 are given in the first two columns of Table 2. For the five partial penetration welds the average DC level was 271 ± 1 mV, while the average DC level of the five full penetration welds was 249 ± 3 mV. As expected, the range of average DC levels lie within the average of the AC variation (Table 2). The small dip at the start of each weld resulted from a gap between a piece of scrap and the plate to be welded, consistent with the sensitivity of the weld monitor to fit-up defects.

Welds made on 1020 steel one week apart were sectioned to test the stability of the correlation between the weld monitor signal and the weld penetration depth (Fig. 1a). The data from both weeks lie along the same correlation curve, indicating the stability of the sensor. The weld monitor output is reliable predictor of penetration, especially if the achievement of partial or full penetration is the primary concern.

The signal from the weld monitor consists of a DC voltage modulated by an AC component. The magnitude and frequency of change in the signal indicates penetration depth, weld defects, and surface contamination. Many commercially available data acquisition and analysis packages are available for use with the weld monitor.

To determine weld penetration from the weld monitor signal, a calibration curve is required. This curve can be constructed for a particular component from test welds made by varying the laser power level at constant speed. After sectioning and polishing, the weld penetration can be measured and correlated with the DC signal from the weld monitor. Using the design specifications for the component of interest, upper and lower control limits could be determined for process monitoring.

If determination of a calibration curve is too difficult or costly, statistical methods can be used to establish the control limits. Weld monitor signals can be collected from a statistically significant number of welds, and this data can be used to establish an envelope of process conditions in which acceptable welds are produced. It is particularly easy to distinguish between partial penetration and full penetration welds, since there is an abrupt drop in the infrared signal emitted above the weld when full penetration is achieved.

Conclusions

The primary infrared signal collected by the weld monitor is linearly related to the penetration depth in partial penetration welds. Full penetration is signified by a significant drop in the DC level of the signal, as well as an increase in the AC component. The weld monitor signal has been shown to increase with penetration for welds from 0.5 to 5 mm deep, although decreased sensitivity was observed at the larger penetration depths.

Part misalignment in rotary welds is manifested by a wavy appearance in the weld monitor output, while surface contamination can lead to significant changes in the AC variation. The day to

day repeatability of the weld monitor is excellent. In addition, welds made a week apart were found to correlate with the same weld penetration curve.

The weld monitor seems to be ideal for tailor blank welding. It is very sensitive to penetration depth, especially detection of full penetration. Part misalignment and oil contamination leads to significant variations in the weld monitor output.

Acknowledgments

This work was funded by the U.S. Department of Energy, Office of Energy Research Laboratory Technology Research Program and the Office of Transportation Technologies. The authors appreciate the collaboration of Spawr Industries and USCAR Low Emissions Partnership in the development of the weld monitor for automotive manufacturing applications. K. H. Leong and B.V. Hunter are co-inventors of the weld monitor. Spawr Industries of Lake Havasu, AZ incorporated weld monitors into the optics for both the CO2 and Nd:YAG lasers and is the exclusive source for inline weld monitors for CO_2 laser applications.

References

1. Chen, H. B., Li, L., Brookfield, D. J., Williams, K., and Steen, W. M. (1991). Laser process monitoring with dual wavelength sensors. In: *Proc. ICALEO 91*, San Jose, CA. Orlando, FL: Laser Institute of America, SPIE **1722,** pp. 113-122.

2. Bagger, C., Miyamoto, I., Olsen, F., and Maruo, H. (1991). On-line control of the CO2 laser welding process. In: *Beam Technology Conference Proceedings*, Karlsruhe, Germany, March 13-14, DVS-Berichte **135,** pp. 1-6.

3. Olsen, F. O., Jørgensen, H., Bagger, C., Kristensen, T., and Gregersen, O. (1992). Recent investigations in sensorics for adaptive control of laser cutting and welding. In: *Proc. LAMP 92*, Nagoka, Japan: High Temperature Society of Japan, pp. 405-414.

4. Chang, D. U. (1994). Monitoring laser weld quality in real time. *Indust. Laser Rev*. 15-16, November.

5. Maischner, D., Drenker, A., Seidel, B., Abels, P., and Beyer, E. (1991). Process control during laser beam welding. In: *Proc. ICALEO 91*, San Jose, CA. Orlando, FL: Laser Institute of America, SPIE **1722**, pp. 150-155.

6. Mori, K., and Miyamoto, I. (1997). In-process monitoring of laser welding by the analysis of ripples in the plasma emission. *J. Laser Appl.*, **9** 155-159.

7. Nava-Rüdiger, and Houlot, M. (1997). Integration of real time quality control systems in a welding process. *J. Laser Appl.*, **9** 95-102.

8. Leong, K. H. (1997). Low cost laser weld monitoring system. In: *Automotive Laser Applications Workshop 1997*, Novi, MI, March 4-5, University of Michigan.

9. Steen, W. M. (1991). *Laser Materials Processing*, London: Springer Verlag.

10. Smithells, C. J., Brandes, E. A., and Brook, G. (1991). *Smithells' Metals Reference Book*, Boston: Butterworths.

11. Forsythe, W. E. (1959).*Smithsonian Physical Tables*, Washington: Smithsonian Institution.

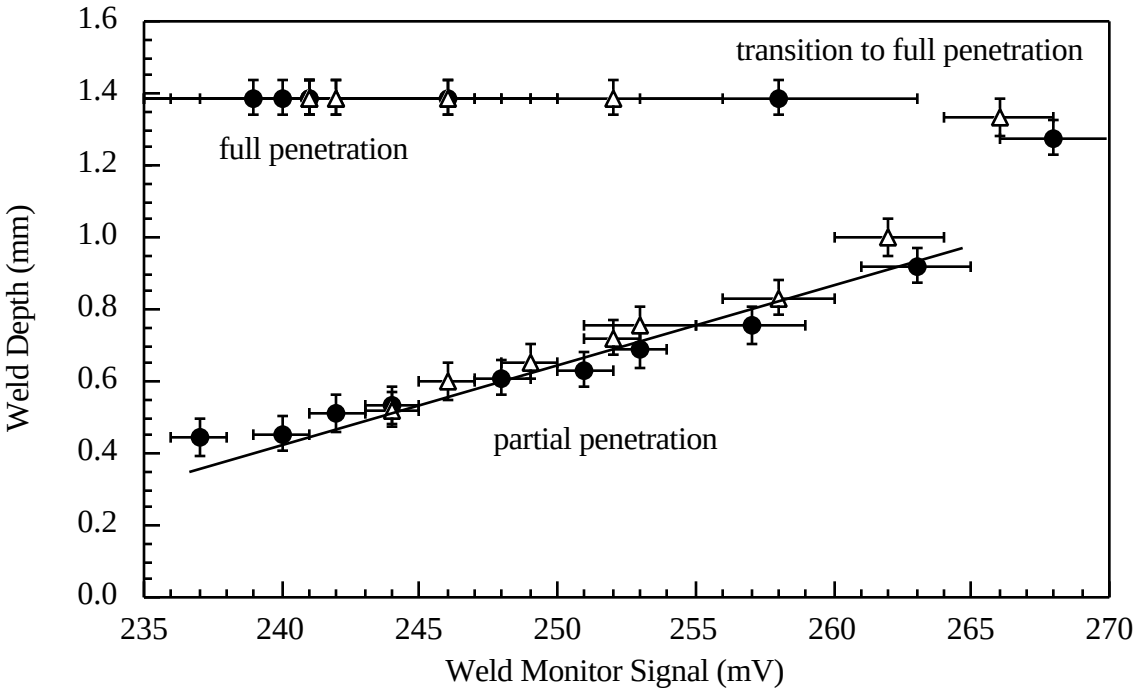
transition to full penetration
full penetration
partial penetration
Weld Depth (mm)
Weld Monitor Signal (mV)
1.6
1.4
1.2
1.0
0.8
0.6
0.4
0.2
0.0
235
240
245
250
255
260
265
270

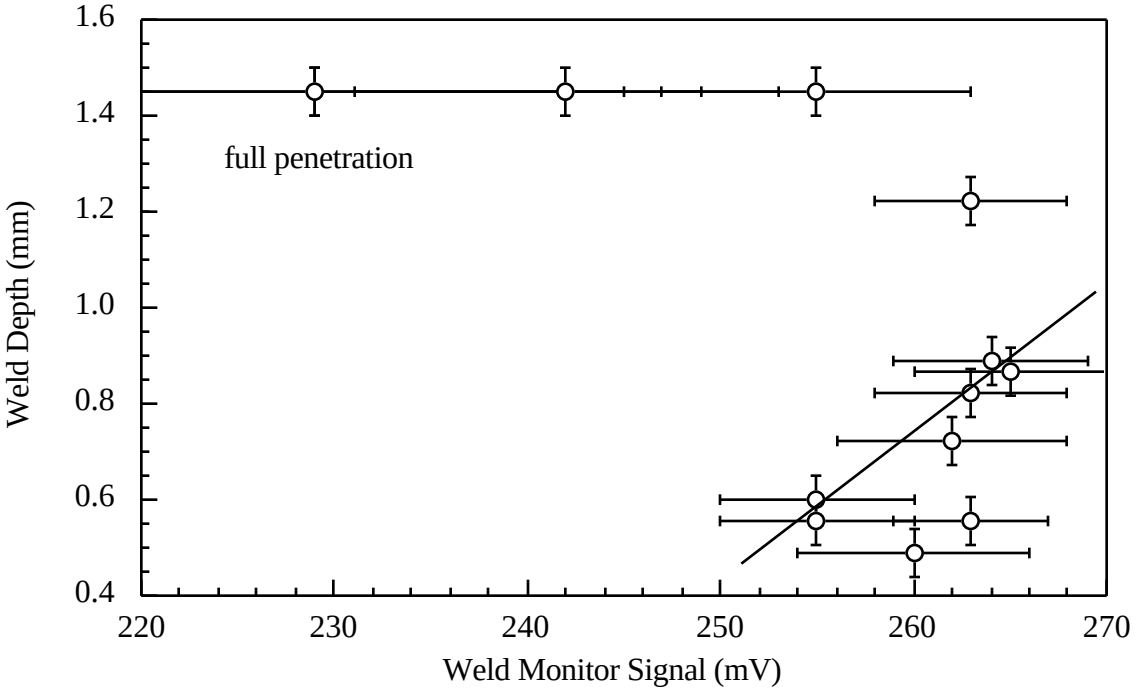
full penetration
Weld Depth (mm)
Weld Monitor Signal (mV)
1.6
1.4
1.2
1.0
0.8
0.6
0.4
220
230
240
250
260
270

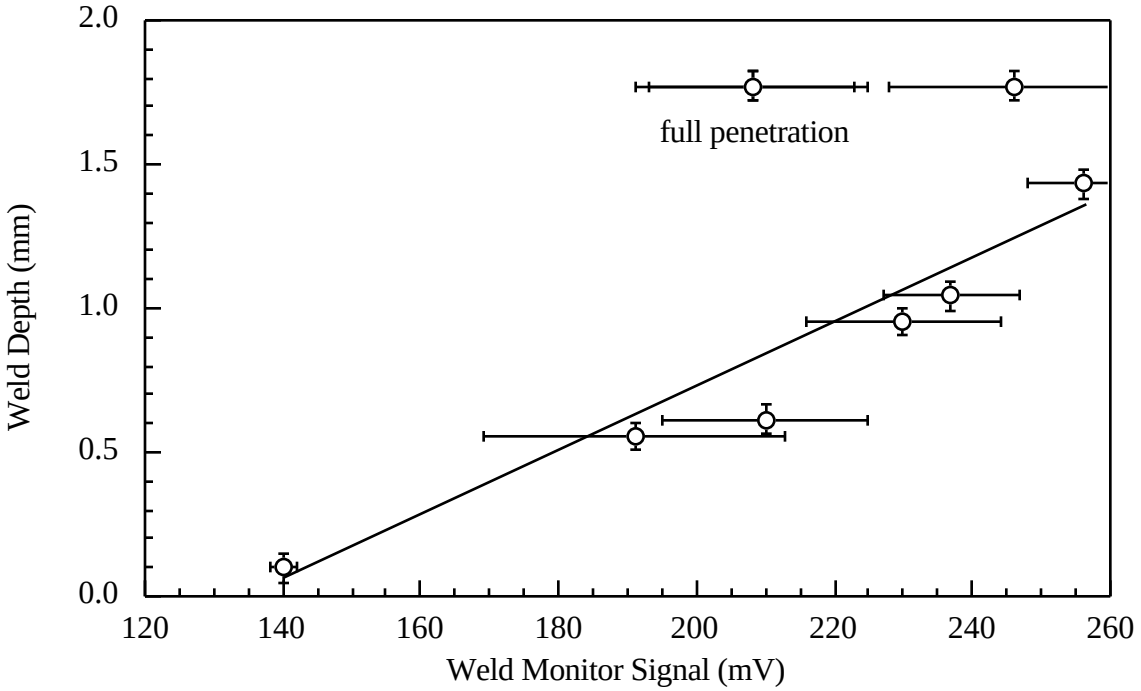

Fig. 1. Correlation between weld monitor DC level and penetration depth for bead on plate welds made with a CO_2 laser on (a) 1020 steel, (b) 6061 aluminum, and (c) AZ31B magnesium. The steel and aluminum penetration were increased by decreasing the travel speed, while the magnesium penetration was increased by increasing the power. The two sets of data shown in (a) were collected 7 days apart to illustrate the weld monitor repeatability.

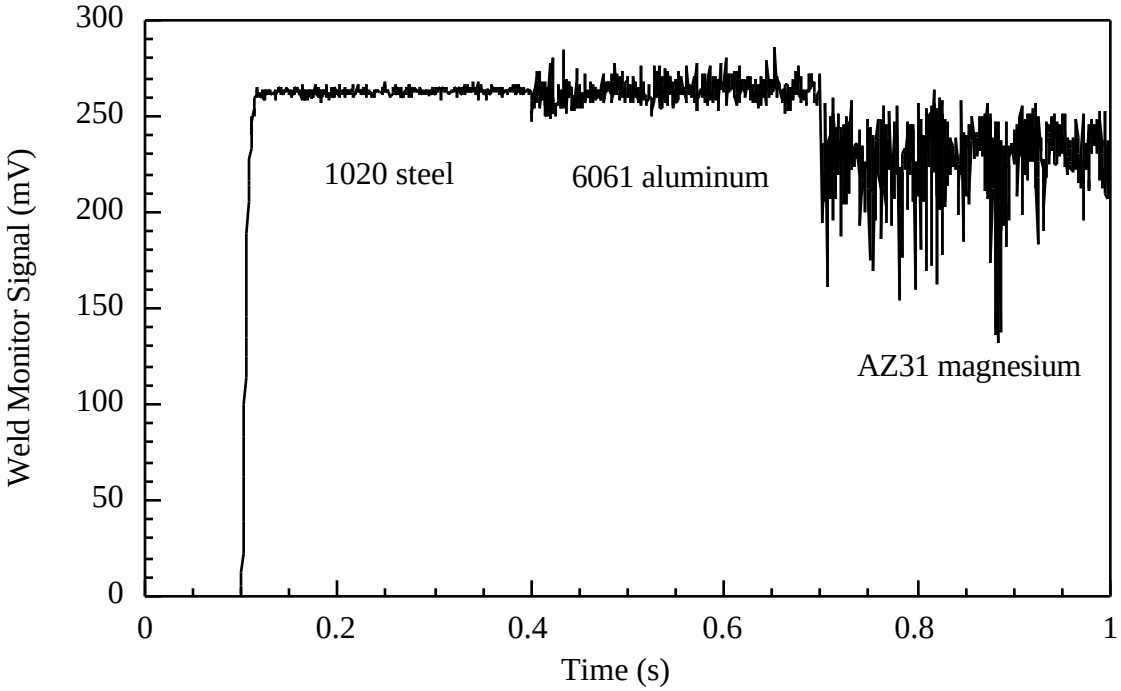

Fig. 2. Differences in the weld monitor signal from 1020 steel, 6061 aluminum, and AZ31B magnesium. For all bead on plate CO_2 laser welds, the penetration depth was ≈ 1 mm and the travel speed was ≈ 13 cm/s. The power was 3.7 kW for the steel and aluminum and 1.2 kW for the magnesium.

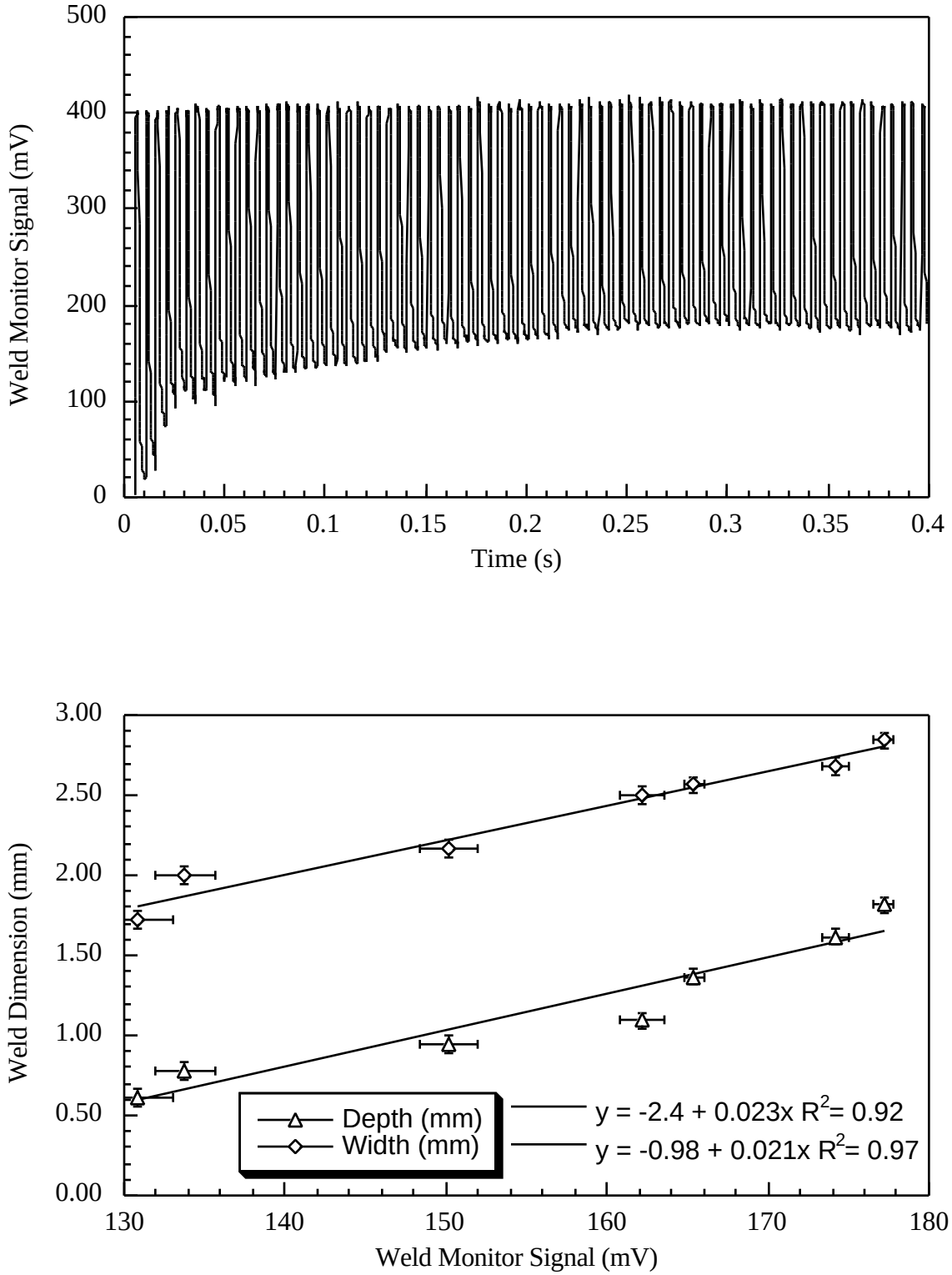

Fig. 3. Weld monitor signal (a) and weld monitor signal correlation with weld depth and width (b)

for bead on plate Nd:YAG laser welds on 1045 steel. The weld monitor signal plotted in (b) was from the lower bound of the signal in (a). The penetration was varied by changing the travel speed at constant power.

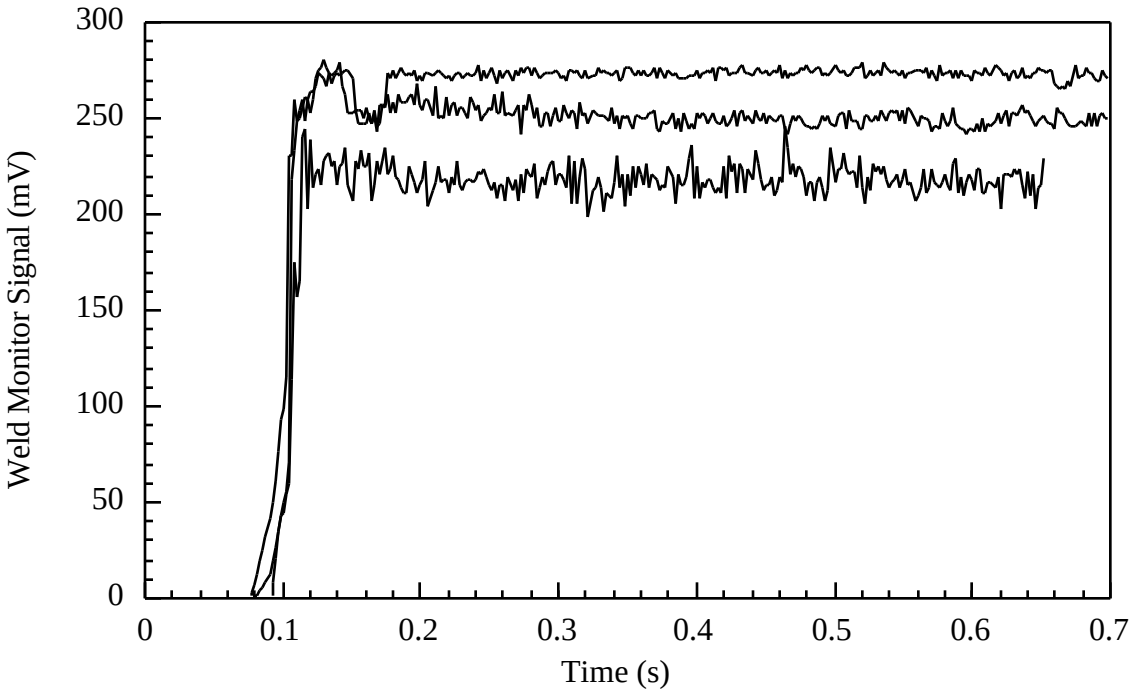

Fig. 4. AC fluctuations of weld monitor signal for bead on plate CO_2 laser welds. The top signal is a partial penetration weld at 13 cm/s and 4.3 kW, the middle signal is a full penetration weld at 13 cm/s and 4.9 kW, and the bottom signal is a full penetration weld at 6 cm/s and 3.7 kW.

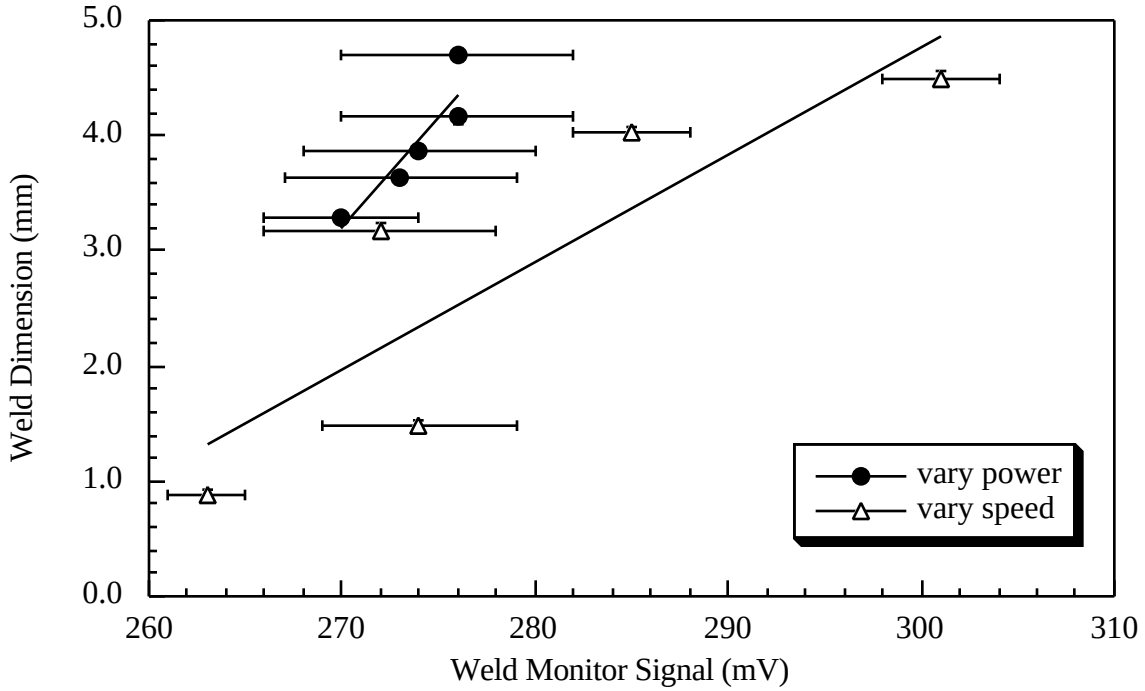

Fig. 5. Weld monitor signal as a function of both travel speed at constant power and and power at constant travel speed for deeper bead plate welds made in 1045 steel with the CO_2 laser. Both curves show a positive trend between the weld monitor output and penetration, although the correlation is not as strong as at lower penetration depths.

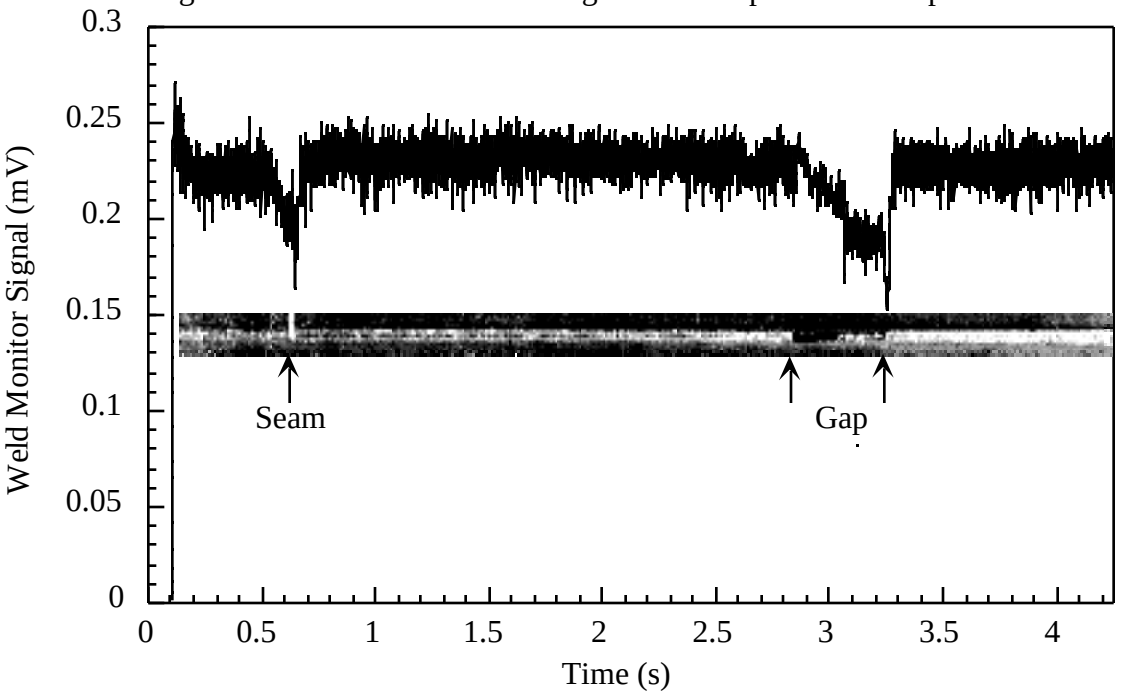

Fig. 6. Image of CO_2 butt weld in 1020 steel with simulated defects along with the corresponding weld monitor signal. Drops in the weld monitor output correspond with a seam and gap in

the butt weld.

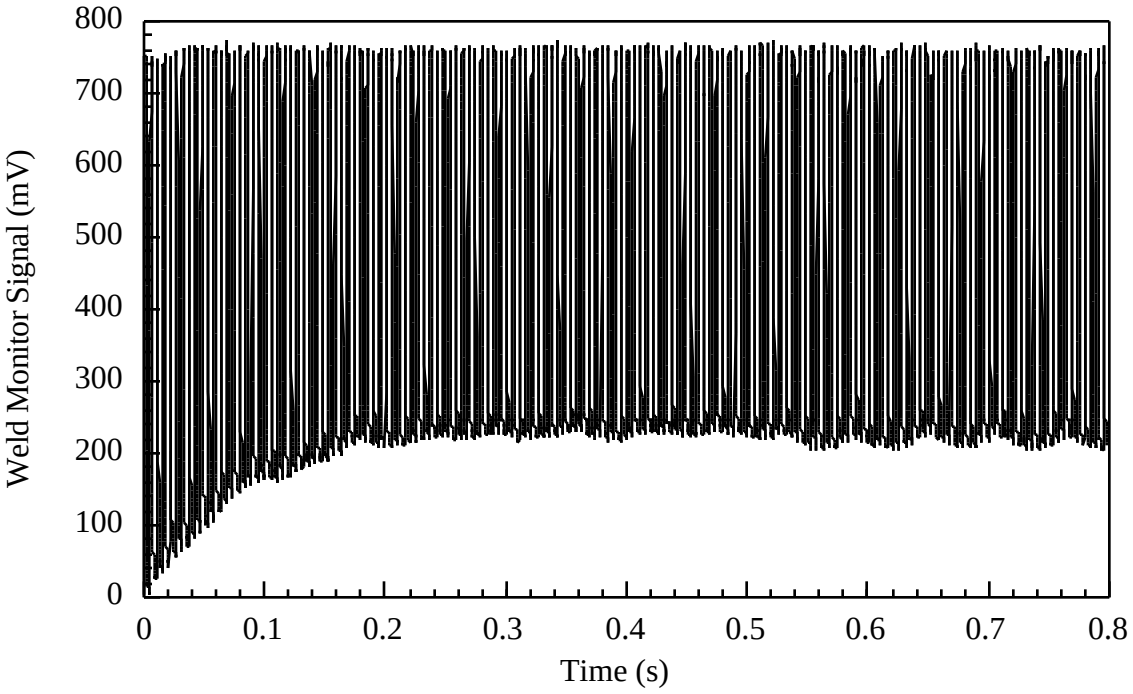

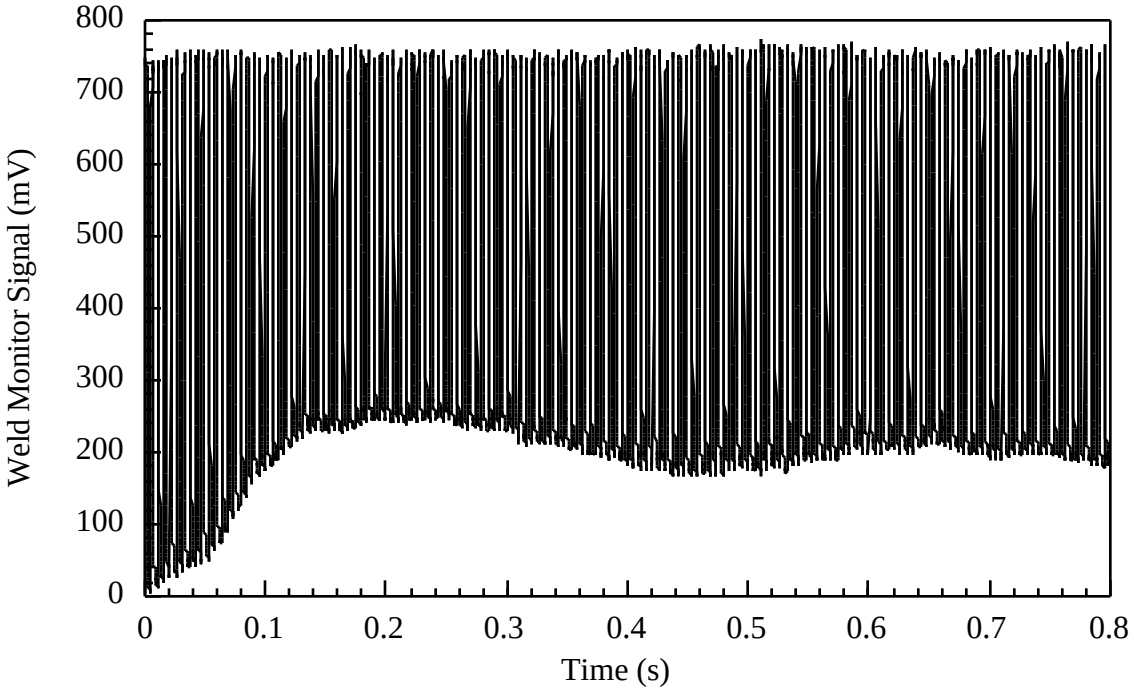

Fig. 7. Weld monitor signal from a Nd:YAG laser weld of a cylindrical fillet joint showing the difference between the weld monitor signals from axially aligned (a) and misaligned (b) parts.

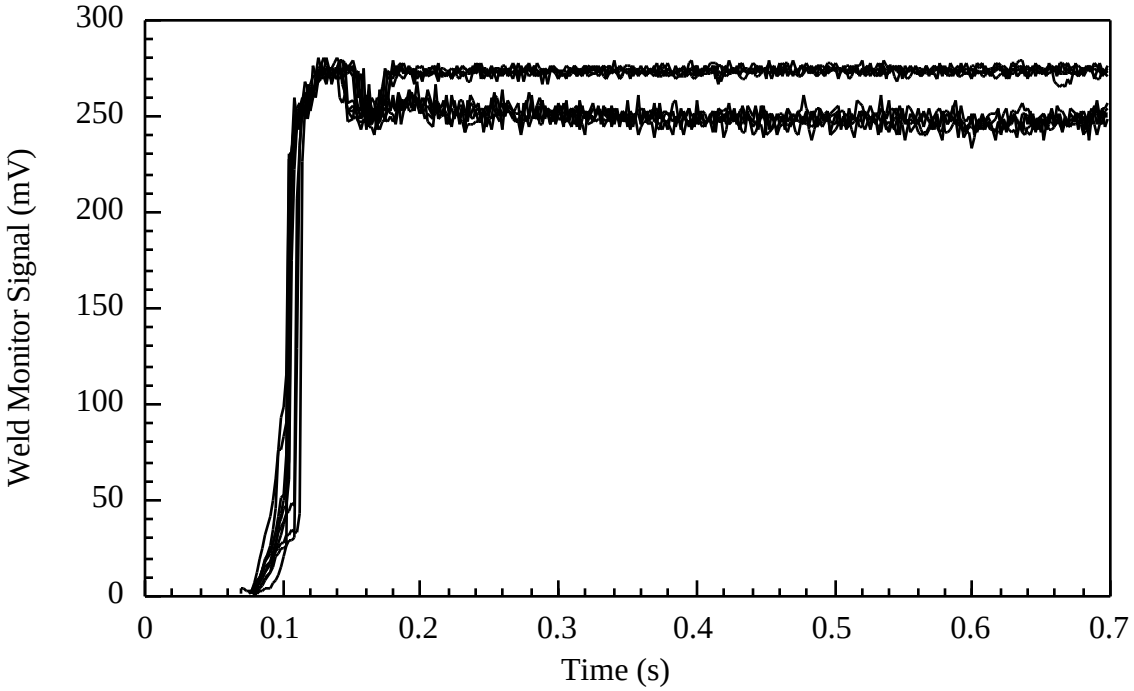

Fig. 8. Repeatability of weld monitor output for full and partial penetration bead on plate CO_2 laser welds on 1020 steel. The plot contains data from 5 partial penetration welds (top) and 5 full penetration welds (bottom). Penetration was v aried by changing the power at constant travel speed.